

Nanoscale

Accepted Manuscript



This is an *Accepted Manuscript*, which has been through the Royal Society of Chemistry peer review process and has been accepted for publication.

Accepted Manuscripts are published online shortly after acceptance, before technical editing, formatting and proof reading. Using this free service, authors can make their results available to the community, in citable form, before we publish the edited article. We will replace this *Accepted Manuscript* with the edited and formatted *Advance Article* as soon as it is available.

You can find more information about *Accepted Manuscripts* in the [Information for Authors](#).

Please note that technical editing may introduce minor changes to the text and/or graphics, which may alter content. The journal's standard [Terms & Conditions](#) and the [Ethical guidelines](#) still apply. In no event shall the Royal Society of Chemistry be held responsible for any errors or omissions in this *Accepted Manuscript* or any consequences arising from the use of any information it contains.

Towards the continuous production of high crystallinity graphene via electrochemical exfoliation with molecular *in-situ* encapsulation

Chia-Hsuan Chen ^{†#}, Shiou-Wen Yang [†], Min-Chiang Chuang [§], Wei-Yen Woon [§] and Ching-Yuan Su ^{†#*}

[†] *Dep. of Mechanical Engineering, National Central University, Tao-Yuan 32001, Taiwan*

[#] *Graduate Institute of Energy Engineering, National Central University, Tao-Yuan 32001, Taiwan*

[§] *Dep. of Physic, National Central University, Tao-Yuan 32001, Taiwan*

To whom correspondence should be addressed: (C. Y. Su) cysu@ncu.edu.tw

KEYWORDS: Electrochemical exfoliation; Graphene; Raman spectroscopy; Transparent conductive film

BRIEFS:

A fast and continuous electrochemical method with melamine additives is able to efficiently exfoliate graphite into high-quality graphene sheets. The hydrophilic force facilitated exfoliation and protection, leading to high yield production of larger size crystallinity of graphene sheets.

ABSTRACT:

Large-scale production of uniform and high-quality graphene is required for practical applications of graphene. The electrochemical exfoliation method is considered as a promising approach for the practical production of graphene. However, the relatively

low production rate of graphene currently hinders its usage. Here, we demonstrate, for the first time, a rapid and high-yield approach to exfoliate graphite into graphene sheets via an electrochemical method with small molecular additives; where in this approach, the use of melamine additives is able to efficiently exfoliate graphite into high-quality graphene sheets. The exfoliation yield can be increased up to 25 wt% with melamine additives compared to electrochemical exfoliation without such additives in the electrolyte. The proposed mechanism for this improvement in the yield is the melamine-induced hydrophilic force from the basal plane; this force facilitates exfoliation and provides *in-situ* protection of the graphene flake surface against further oxidation, leading to high-yield production of graphene of larger crystallite size. The residual melamine can be easily washed away by water after collection of the graphene. The exfoliation with molecular additives exhibits higher uniformity (over 80% is graphene of less than 3 layers), lower oxidation density (C/O ratio of 26.17), and low defect level ($D/G < 0.45$), which are characteristics superior to those of reduced graphene oxide (rGO) or of a previously reported approach of electrochemically exfoliated graphene (EC-graphene). The continuous films obtained by the purified graphene suspension exhibit a sheet resistance of 13.5 k Ω /sq at ~95% transmittance. A graphene-based nanocomposite with PVB exhibits an electrical conductivity of 3.3×10^{-3} S/m for the graphene loading fraction of 0.46 vol %. Moreover, the melamine functionalized graphene sheets are readily dispersed in the aqueous solution during the exfoliation process, allowing for production of graphene in a continuous process. The continuous process for producing graphene was demonstrated, with a yield rate of 1.5 g/hr. The proposed method can produce high-crystallinity graphene in a fast and high-

yield manner, which paves the path towards mass production of high-quality graphene for a variety of applications.

INTRODUCTION:

Graphene, a two-dimensional single atomic layer carbon allotrope,^{1, 2} has attracted significant attention in recent years due to its unique and extraordinary material properties, such as high carrier mobility($\sim 200000 \text{ cm}^2/\text{V.s}$)³, excellent mechanical strength and elasticity, and superior thermal conductivity.^{4, 5} The unique material properties of graphene can potentially be used in a broad range of applications, including frontier nanoelectronics⁶⁻¹⁰, functional nanocomposite^{11, 12}, energy storage^{13, 14}, thermal managements¹⁵, and ultrasensitive chemical/bio-sensors¹⁶. However, realization of these applications requires development of a cost-effective method for producing graphene on an industrial scale. To date, many approaches exist for producing graphene, including mechanical exfoliation^{2, 17}, chemical vapor deposition(CVD),¹⁸⁻²⁰ epitaxial growth,²¹ liquid phase exfoliation,^{22, 23} chemical exfoliation of graphene oxide(GO) and reduced graphene oxide(rGO)^{24, 25}, ball-milling,²⁶ as well as the intercalation and expansion of graphite.²⁷ For some specific applications that require production of large quantities of high-quality graphene on a large scale and at low cost, the use of graphene derived from bulk graphite is considered the most economical method. Among these methods, the chemical exfoliation of GO/rGO and liquid-phase exfoliation are the two main routes for producing large-scale graphene, using either the powder or solution phase; the chemical exfoliation procedure is beneficial for subsequent chemical functionalization and for adapting to a variety of fabrication tools, such as the frequently used rod-coater and air brush technologies. In addition, the solution-phase procedure is

now well developed for the applications of energy storage and nanocomposite materials. Chemical exfoliation methods are based on the Hummers' method,²⁵ in which graphite is first oxidized and then exfoliated into mono-layered graphene oxide (GO) flakes, followed by chemical or thermal reduction.^{28, 29} This procedure has the advantages of low cost and the potential for scaling up to high volume production. However, the oxidation process produces oxidized functional groups, which can severely damaging the honeycomb lattice of graphene. Although the subsequent reduction procedures remove most of these oxidized groups and partially restore the graphitic lattice, a higher defect density remains after the procedure, and the GO sheets typically require a high-temperature (900-1200°C) annealing step to further recover the graphitic structure.^{8, 29} Therefore, the time-consuming nature and the high operating temperature of this method hinder the production of high-quality graphene. In the other hand, the liquid-phase exfoliation technologies are based on extensive sonication of graphite in solvents, such as dimethylformamide (DMF) and methylpyrrolidone (MNP), to weaken the van der Waals forces between the graphite layers.^{22, 23} Although the obtained graphene is of high quality, the low production yield of thin graphene layers and the limitation of the flake size ($<1\mu\text{m}^2$) hinder its commercial usage. Recent works regarding the modified liquid-phase exfoliation approach using a high shear-rate exfoliation in solvent have shown the capability to increase the production rate to ~ 5.3 g/h.²² This scalable procedure to produce ultra-low defect content graphene is beneficial for the industrial production of graphene. However, such graphene sheets are a mixture of various layers, requiring an additional step to separate and extract thin graphene sheets, which is time consuming. Moreover, the small flake size ($\sim 300\text{-}800$ nm in lateral size) due to the intensive blend

in grinder, hinders its usage on specific application such as transparent conductive film and nanocomposite.

Recently, the electrochemical exfoliation approach has attracted much attention.³⁰⁻³⁴This approach is of low cost, is scalable, and provides fast and easy processing and the ability to produce high-quality graphene with an arrow distribution of layer numbers(> 60% belong to 2-3 L), as well as larger flake size (up to ~30 μm).³⁴ The mechanism of this approach is based on the intercalation of the graphite layers using various intercalatants (e.g., SO_4^{2-}) placed into the space between layers, followed by expansion and subsequent exfoliation of graphene. The reported works involving electrochemical exfoliation consider various types of electrolytes, such as ionic liquid and aqueous acid(e.g., H_2SO_4 , HNO_3 , and H_3PO_4) as well as inorganic salts(e.g., Na_2SO_4 or K_2SO_4),³² to exfoliate graphite. Recent work by employing sulfonate salts as electrolyte or additives, such as sodium dodecyl sulfate(SDS)³⁵, sodium dodecyl benzene sulfonate (SDBS) and cetyltrimethylammonium bromide (CTAB)³⁶, have demonstrated the success for graphene exfoliation due to that the additives plays both role for stabilizing surfactant and intercalant during the electrochemical exfoliation. Although the obtained graphene exhibits superior electrical conductivity compared to rGO, the oxidized functional groups cannot be further removed due to the acid functionalization of graphene. Moreover, the electrochemical exfoliation approach suffers from a relatively low production yield for each batch procedure, which is mainly attributed to its non-continuous process and inefficient exfoliation procedure; this inefficient exfoliation is partially due to the exfoliated graphene being segregated onto the graphite surface and saturating the electrolyte activity during long-term processing, which degrades the

electrochemical intercalation and exfoliation process. Thus far, most of the relevant works in the literature lack a method to prevent the surface oxidation of graphene; as a result, a high defect density cannot be avoided. Additionally, the process uses graphite-bulk or graphite rods as raw materials; unlike graphite powder, the higher cost and lack of ease of self-filling prevents the electrochemical exfoliation approach from achieving the continuous production mode. Moreover, the electrolyte cannot stabilize the exfoliated graphene during the process, thus hindering the continuous collection of as-exfoliated graphene.

In this work, we demonstrate a conceptually continuous electrochemical method for the exfoliation of graphite powder using a modified electrolyte with melamine additives. The procedure enables an increase of the production yield to ~20 wt % with a lower defect density. The melamine derivatives serve multiple purposes during this process. First, the NH_2 groups of melamine exhibit extensive interaction with the graphene surface, forming a hydrophilic force normal to the graphene basal plane, which facilitates the exfoliation of graphite. Second, the as-exfoliated graphene is *in-situ* encapsulated by the melamine molecular, preventing further oxidation from acid species, thereby maintaining the high graphitic networks of graphene. Third, the melamine-modified graphene exfoliated from graphite readily forms a stable dispersion, which promotes subsequent collection and purification. Using this modified process, graphene sheets with the highest C/O ratio of 26.1 (oxygen content of 3.68 atom %) and a large crystalline size of 36.2 nm were obtained. A transparent conductive film made using these graphene flakes exhibits a conductivity of 13.6 kOhm/sq (at T: 95.2 %), which is superior to the conductivities of rGO and electrochemically exfoliated graphene films.⁸ The properties of high-efficiency production in a continuous manner of the melamine-

modified method allow for an increase of the production yield as high as 1.5 g/hr. The graphene-based polymer composites (graphene/PVB) exhibited an electrical conductivity of 3.3×10^{-3} S/m at a loading fraction of 0.4 vol%. Overall, our findings not only shed new light on the fast and continuous production of graphene but also provide a new strategy to obtain excellent-quality graphene via molecule-assisted exfoliation and *in-situ* encapsulation. This fast and cost-effective approach paves the way to practical large-scale production of high-quality graphene.

RESULTS AND DISCUSSION

In this work, the electrochemical exfoliation of graphite was performed in an electrolyte comprising sulfuric acid and various amounts of melamine additives. Figure 1a illustrates the experimental setup, in which high-crystallinity bulk graphite was used as the electrode and the source material for electrochemical exfoliation of graphene. Two graphite electrodes were placed parallel to each other with a separation of 8 cm. The electrolytes were based on aqueous acids (H_2SO_4 in DI water) with various melamine additives (see supporting materials S1 for the details). For example, H_2SO_4 solution (mixture of 6.5 g of 98% H_2SO_4 were diluted in 100 mL of DI water) with melamine additives of 20 mL/10 mL was used as the electrolyte. The static voltage bias was ramped from 0 V to +20 V on the graphite electrode. As demonstrated in our previous work,³² the long-term operation of a single step voltage normally leads to highly oxidized graphene sheets. To avoid long-term oxidation, the optimized procedure was modified to apply the voltage for 5 min, and then the voltages were applied by alternating between +20 V and -20 V, until the desired amount of graphene sheets was obtained. Figure 1b shows the electrochemical exfoliation process after 5 min and 15

min. When the graphite was subjected to static voltage, it began to expand and then became dissociated. We noticed that the electrochemically exfoliated graphene with melamine additives is highly efficient and the as-exfoliated graphene sheets can be readily suspended in electrolyte solution (Figure 1c). The exfoliated products were washed with a large amount of DI water until the pH value reached ~7.0; they were then collected using a 100 nm porous filter and dried. The amount of exfoliated graphene with melamine additives was 20.3 wt% greater than that of the case without the additives, indicating that melamine molecules can efficiently facilitate the exfoliation of graphene from graphite. From the viewpoint of molecular functionalization, a plausible mechanism is proposed to explain this phenomenon. Figure 2 schematically illustrates the exfoliation mechanisms with and without melamine in the electrolyte. On one hand, in the case of the electrolyte without melamine; when the graphite is subjected to static bias, the sulfate ions (SO_4^{2-}) gradually intercalate into the graphite interlayer spacing and directly functionalize the graphene basal plane, leading to severely oxidized graphene sheets. On the other hand, for exfoliation using the electrolyte with melamine additives, the melamine molecules were spontaneously absorbed on the graphite basal plane due to the extensive interaction of their NH_2 groups and the π - π interaction between graphene and melamine. During the exfoliation process, the sulfate ions began to intercalate into the graphite, resulting in a hydrophilic force (normal to the basal plane) from the graphite surface, thereby facilitating the exfoliation of the top graphene sheets from the graphite. Moreover, the as-exfoliated sheets were *in-situ* encapsulated with melamine molecules, thereby preventing further oxidation due to the acid species. By repeating such mechanisms, the encapsulated graphene can be subsequently exfoliated from the graphite and readily dispersed into the electrolyte due to the high solubility of melamine

in water. The final product can be collected and purified with DI water and then dried for further characterizations.

Figure 3a shows the morphology of the as-prepared graphene as determined by scanning electron microscopy (SEM). The magnified image shown in Figure 3b reveals the clean surface of graphene with winkle features, suggesting that the obtained graphene sheets were thin and of high purity, without many contaminants. The results of energy-dispersive X-ray spectroscopy (EDS) characterization (see supporting Figure S2 for details) indicate that the amount of impurities is less than 1.2 %. Transmission electron microscopy (TEM) was used to evaluate the crystalline quality of the as-prepared graphene sheets and the graphene. Figure 3c shows the typical TEM image for the exfoliated graphene sheet, which appears continuous and of uniform thickness over a large area. The corresponding selected area electron diffraction pattern (SAED) exhibits a typical hexagonal diffraction pattern, indicating the high crystalline quality of the graphene sheet. Figure 4a shows a typical optical image for the obtained graphene sheet on a clean SiO₂ substrate. The average lateral size of sheet was approximately 18 μm, which is significantly larger than that of the graphene sheet obtained by shear or liquid-phase exfoliation methods. The representative AFM image for a graphene sheet shows a mean thickness of 1.76 nm (Figure 4c), indicating that the graphene sheets are a few layers (<3 layers) in thickness. The thickness distribution was studied by statistical analysis for 45 graphene sheets (Figure 4d), revealing that over 90% of the sheets were less than 3.5 nm in thickness.

During the exfoliation procedure, the melamine molecules *in-situ* absorb onto the graphene surface, which facilitates the exfoliation of graphite and promotes stabilization of the as-exfoliated sheets in the electrolyte. Melamine was found to be readily washed

away from the products by DI water. XPS characterization was used to confirm the amount of contamination due to N atoms on graphene after being washed. Figure 5a shows the correlation between N content and washing cycles, indicating the fact that the N content was less than 0.96 at% when subjected to five cycles of flushes.

Figure 5b shows the Raman spectra for the starting material of bulk-graphite and the exfoliated graphene sheet with and without melamine additives. Note that the selected graphene sheets analyzed here were of a thickness lower than 1.8 nm by AFM characterization (on SiO₂/Si substrate). The indicated G peak (at ~1580 cm⁻¹) and the 2D peak (at ~2700 cm⁻¹) are characteristics of the *sp*² C=C bonds (graphitization) in graphene.³⁷⁻³⁹ The D peak (at ~1350 cm⁻¹) is related to non-*sp*² carbon bonding, such as that of lattice disorder, structure defect, or functional group bonding.^{40, 41} The case without melamine clearly shows a remarkably intensified D peak, indicating the introduction of lattice disorder. Moreover, the G peak width is broadened, and its shoulder D' peak (at ~1623 cm⁻¹) is pronounced, which is attributed to the intra-valley resonance of phonon scattering,⁴² indicating that the *sp*³ carbon bonding is likely due to the oxygen functionalized groups in acid solution during the electrochemical exfoliation. In contrast, the exfoliation with melamine additives shows a lower-intensity D' peak, and the intensity ratio of the D and G peaks ((I(D)/I(G))) is ~0.20-0.54, which is much smaller than that without melamine additives (~0.41-0.92) (Figure 5c) and reduced GO (~1.1-1.5),⁴³ suggesting that the low defect density of graphene can be obtained with the use of the additives of melamine. Moreover, the 2D/G ratio has been shown to be related to the recovery degree of *sp*² C=C bonds. The 2D/G for the case of melamine additives (~0.25) is higher than that with typical electrochemical exfoliation process (~0.20) and is significantly higher than those of reduced GO, indicating the high

degree graphitization of the carbon network. From Figure 5d, we estimated the crystallite size (L_a) and the distance (L_d) between lattice defects of the graphene basal plane.⁴⁴⁻⁴⁶ The L_a varies inversely with the acquired $I(D)/I(G)$ from the Raman spectrum: $I(D)/I(G)=C(\lambda)/L_a$, where $C(\lambda)$ is the constant related to the excitation wavelength used in the Raman spectrum.⁴⁶ The estimated L_a for the case with melamine additives is 36.3 nm on average, which is higher than that of the case of the electrolyte without melamine(16.4 nm) or the highly reduced GO(\sim 1-4 nm)²⁹, and this value is comparable to that of the high-quality noncovalently modified graphene obtained via the ball-milling approach.²⁶ In addition, the L_d for melamine(16.7 nm) is higher than that without additives(11.1 nm), suggesting the low defect density and higher graphitization of crystalline graphene. The XPS characterization data shown in Figure 5e,f of the C1s binding energy profile proves that there exist fewer oxygen-containing functional groups(such as C-OH(285.2 eV), C=O(286.7 eV) and COOH(289.8eV)) for the as-prepared graphene with melamine, which is consistent with the aforementioned higher crystalline size of graphene. The calculated C/O ratio of 26.7(i.e., oxygen content of 3.6 atomic %) for the case of melamine is significantly higher than that of electrolyte without additives(15.98) and those reported for rGO and electrochemical exfoliated graphene.^{32, 34, 47} Moreover, the XRD patterns on exfoliated graphene were characterized as shown in Figure S4. It is clearly seen that a sharp and high intensity peak (002) at about 26° were observed for graphite(raw materials), indicating very high degree of crystallinity with a derived interlayer spacing of 0.334 nm. On the other hand, the XRD pattern on the exfoliated graphene shows a relative broad peak at about 25.7° , indicating the high crystallinity of exfoliated graphene with interlayer spacing of 0.345 nm. The result represent the exfoliated graphene by this approach is of high quality. The observed highly crystalline graphene obtained using the method with melamine additive is attributed to the

aforementioned mechanism, where the *insitu* encapsulated graphene, by melamine molecules during the electrochemical exfoliation process, prevents the further oxidation from the acid species.

To confirm the graphitic structure in as-exfoliated graphene by melamine additive electrolytes, the transparent conductive film (TC film) was made on a quartz substrate to evaluate the electrical properties. In brief, the transparent graphene film was prepared by a graphene suspension at a concentration of 0.2 mg/mL in DMF, followed by a self-assembly and drying process, as reported in previous work.³⁴ Figure 6a shows the photograph and optical image of graphene film on a substrate, where the graphene flakes are interconnected with intersheet junctions to form a percolation-type thin film. The samples of various conditions for study here were selected to have an optical transparency of $\sim 95.2\%$ (at 550 nm) by this simple self-assembly approach. The measured sheet resistance values for various thin films are shown in Figure 6b. The sheet resistance for the thin film made from melamine-derived graphene is $\sim 21.8\text{ k}\Omega/\square$, which is clearly lower than that of the thin film obtained via a conventional electrochemical exfoliation process ($\sim 138\text{ k}\Omega/\square$).³⁴ The observed properties are consistent with the aforementioned arguments from the Raman scattering study and the XPS analysis, where the melamine-derived graphene preserved its high graphitic structure, which is beneficial for increasing electrical conduction. Moreover, the graphene with AuCl_3 doping is considered to be stable and represents a promising approach for lowering the electrical resistance of graphene due to the increase of the hole carrier concentration.⁴⁸ In this case, the sheet resistance of the AuCl_3 -doped graphene film can be further lowered to $\sim 13.5\text{ k}\Omega/\square$ while maintaining its high optical transmittance (i.e., $\sim 95\%$).

For particular applications, graphene, with its combination of extraordinary material properties and its ability to be blended into various polymers, can be used to create a variety of graphene/polymer nanocomposites that exhibit favorable electrical, thermal, and mechanical properties. For example, graphene sheets can create a percolated pathway for electron transport in a composite, thus making graphene/polymer composites electrically conductive.⁴⁹ However, the conductivity significantly depends on the loading amount of graphene and the graphene flake size as well as the uniformity of dispersion of graphene in the polymer matrix. The reported works using extensive functionalization of graphene with oxidized groups (i.e., epoxide and hydroxyl groups in rGO) greatly facilitate the dispersion of graphene in polymers. However, the extensive functionalization significantly degrades the high conductivity nature of graphene, thus lowering the electrical conductivity of the composite. In our works, the prepared graphene with high electrical conductivity and moderate oxygen groups on the graphene in-plane is a suitable candidate for the formation of nanocomposites of high electrical conductivity. Figure 7 shows the graphene-based nanocomposite using a solvent-based strategy to disperse graphene in polyvinyl butyral (PVB). PVB has the advantages of mechanical elasticity, sound dampening property, and the ability to protect of interiors from fading. However, PVB is an electrical insulator by nature. Here, we modify PVB to be electrically conductive via the addition of graphene. The PVB and as-prepared graphene can each be well dispersed in N-Methyl-2-pyrrolidone (NMP), and then, the two mixtures can be blended to form a graphene/PVB suspension in NMP, as shown in Figure 7a (see the experimental section for details). The nanocomposite film with a thickness of $\sim 60 \mu\text{m}$ was obtained by casting, followed by drying. The electrical conductivity of the film is $3.3 \times 10^{-3} \text{ S/m}$, corresponding to the electrical percolation

threshold, with a graphene volume fraction of 0.46 vol%. Figure 7c,d shows the SEM images, where the graphene flakes were uniformly distributed and embedded in the matrix polymer. The electrically conductive nanocomposites prepared with our high-quality graphene can potentially be used for electromagnetic and anti-electrostatic coatings and conductive paints or as functional materials for 3D printing.

Another issue for the current limitation of graphene fabricated using the electrochemical exfoliation approach is the low production yield and the lack of the ability to be implemented in the continuous process required for industry usage. As mentioned in a previous section, the melamine additives in the electrochemical exfoliation process result in a hydrophilic surface on graphene, allowing for the exfoliated graphene sheets to be readily well dispersed in aqueous solution. Therefore, our process can be further modified to be used in a continuous production setup. Figure 7a illustrates the experimental setup for this continuous production concept, where the starting materials of bulk graphite are replaced by a piston-operated container filled with natural graphite powder (~20 g). Note that there was a Nylon filter (75 mesh) encapsulating the bottom of the container to ensure that the electrolyte is able to flow through the filter and into the graphite powder. Figure 7b shows the evolution of this process: first, the graphite powder was subjected to a static bias of 20 V for 10 min. Next, the voltage bias was turned off, followed by the operation of the piston to complete one cycle. The exfoliated graphene flakes were clearly extracted out through the underlying filter from the container when the piston cycle was operated. After continuous processing for 30 min, the graphene suspension was collected via filtration and purification. Figure 7c shows the image of the obtained graphene powder and its suspension in NMP solution. The production yield is estimated to be 1.5 g/hr, which is comparable to that of most of the liquid-based exfoliated approaches; however, our approach maintains a larger flake size (15~30 μm) than these previously reported approaches. Table S2 compares our method with other reported approaches. The quality

and production yield is an order of magnitude higher than that of rGO. The C/O ratio and yield are comparable to those of most of the liquid phase exfoliation approaches, while the flake size is 100 times larger. These results demonstrate that the melamine additives in a modified electrochemical exfoliation approach can be used in a continuous process and for a high production rate of high-quality graphene, which paves the way for industrial-scale graphene synthesis for various applications in the future.

CONCLUSIONS

In conclusion, a rapid and continuous electrochemical method with melamine additives in the electrolyte was demonstrated to efficiently exfoliate graphite into high-quality graphene sheets. The melamine-induced hydrophilic force from the basal plane facilitates the exfoliation of graphene and provides *insitu* protection of the graphene flake surface to avoid further oxidation, leading to high yield and larger crystallite size of the graphene sheets. The obtained graphene sheets are of high quality, with a C/O ratio of 26.1 and a crystalline size of 36.2 nm. The TC film composed of graphene sheets exhibit a conductivity of $\sim 13.5\text{K ohm/sq}$ at 95% transparency. The graphene/PVB nanocomposite exhibits a conductivity of $\sim 3.3 \times 10^{-3} \text{ S/m}$ at matrices of 0.4 vol%. Moreover, for the first time, a continuous production setup, using graphite powder as the starting material, was demonstrated to provide a production yield of $\sim 1.5 \text{ g/hr}$, which is significantly higher than the yields reported for other electrochemical exfoliation methods. This work provide a novel strategy to obtain high-quality, larger-size graphene sheets using a continuous production approach, which addresses the current issue of low yield of graphene production via the electrochemical exfoliation approach.

EXPERIMENTAL SECTION

Electrochemical Exfoliation process :

For the description of the basic setup for preparing graphene via the electrochemical exfoliation method, please refer to our previous work.³⁴ In this present method, bulk graphite and graphite powder (Chuetsu Graphite Works Co., Ltd.; 20 mesh) were used as the starting materials for producing graphene. The ionic solution was prepared by taking 6.5 g of sulfuric acid (Sigma-Aldrich; 98%) and diluting it in 100 mL of DI water. To study the effect of melamine-assisted graphene exfoliation, 10–200 g of melamine (Alfa Aesar; 99%) was added into the electrolyte. The electrochemical exfoliation process was performed by applying an alternating DC bias of ± 20 V (the current is ~ 3 A) for 10 min on each electrode. The graphene sheets were collected by vacuum filtration with a 100 nm filter and then washed with 5 cycles (total 3 L) of DI water to remove the acid species and melamine residuals. After drying, the graphene powder was suspended in DMF or NMP and further dispersed in water-bath sonication for 5 min. To remove the unwanted graphite particles produced during the exfoliation, the suspension was subjected to centrifugation at 3000 rpm for 30 min. The upper portion was extracted for subsequent characterization studies and to be used in applications. Here, the production yield was estimated by the weight ratio of the purified graphene powder to the consumed graphite. To screen out these un-reacted graphite particles, the purified graphene powder was obtained using a process of dispersion, centrifugation and freeze drying. The production rate was estimated by the ratio of the amount of graphene powder to the processing time (g/hr).

Preparation of transparent conductive films:

Prior to graphene film deposition, the receiving quartz substrates were first cleaned with a Piranha solution to make the surface hydrophilic. Approximately 500 μ L of graphene suspension with a concentration of 0.2 mg/mL in DMF was dropped onto the substrate

surface, followed by dropping of 300 μ L of DI water. The thin graphene films were observed to become self-assembled at the solution surface. Next, the sample was dried in a fume hood overnight, followed by baking at 120 $^{\circ}$ C for 1 hr to remove the residual DMF. Regarding the AuCl₃-doped graphene film, gold chloride powder(Sigma-Aldrich; 99%) was first dispersed in nitromethane(Alfa Aesar; 98%) to form a 30 mM solution(0.182 g in 20 mL). The solution,200 μ L in volume, was dropped onto the graphene film and allowed to rest for 1 min, followed by spincoating at 3000 rpm to remove the residual solution.

Preparations of graphene/PVB nanocomposite:

To prepare the graphene/PVB nanocomposite, 0.1 g of PVB powder was mixed with 5 ml of NMP solvent using a magnetic stirrer and kept at 80 $^{\circ}$ C until the powder was completely dissolved in the solvent. Next, the graphene suspension(1 mg/5 mL in NMP) was added into the PVB/NMP solution, followed by water bath sonication of the mixture for 30 min. The prepared mixture solution was then poured into a Petri-dish and baked at 100 $^{\circ}$ C in a vacuum oven for 3 hr. The graphene/PVB composite was then peeled off the dish.

Characterization:

The AFM images were obtained using a Veeco Dimension-Icon system. Raman scattering spectral analysis was performed using a Horiba HR 550 confocal Raman microscope system (laser excitation wavelength = 532 nm; laser spot-size \sim 0.5 μ m). The Raman scattering peak of Si at 520 cm^{-1} was used as a reference for wavenumber calibration. The UV-vis-NIR transmittance spectra were obtained using a spectrophotometer(Hitachi).The chemical configurations were determined using an X-

ray photoelectron spectrometer (XPS, Phi V6000). The XPS measurements were performed using a Mg K α x-ray source for sample excitation. The energies were calibrated relative to the C 1s peak to eliminate the charging of the sample during analysis. The SEM imaging was performed using a JEOL-6330F instrument, and the TEM observations were performed using a JEOL-2010F instrument with accelerating voltage of 200kV. The electrical conductivity measurements were conducted using a four-point-probe system(FPSR100).

Acknowledgements: This research was supported by Natinoal Science Council Taiwan (102-2221-E-008-113-MY3)

Supporting Information Available: The detail process recipe, EDS, results are available. This material is available free of charge via the Internet at <http://pubs.acs.org>

REFERENCES:

1. Novoselov, K. S.; Geim, A. K.; Morozov, S. V.; Jiang, D.; Katsnelson, M. I.; Grigorieva, I. V.; Dubonos, S. V.; Firsov, A. A. Two-dimensional gas of massless Dirac fermions in graphene. *Nature* 2005, 438, 197-200.
2. Novoselov, K. S.; Geim, A. K.; Morozov, S. V.; Jiang, D.; Zhang, Y.; Dubonos, S. V.; Grigorieva, I. V.; Firsov, A. A. Electric field effect in atomically thin carbon films. *Science* 2004, 306, 666-669.
3. Bolotin, K. I.; Sikes, K. J.; Jiang, Z.; Klima, M.; Fudenberg, G.; Hone, J.; Kim, P.; Stormer, H. L. Ultrahigh electron mobility in suspended graphene. *Solid State Commun.* 2008, 146, 351-355.
4. Balandin, A. A.; Ghosh, S.; Bao, W. Z.; Calizo, I.; Teweldebrhan, D.; Miao, F.; Lau, C. N. Superior thermal conductivity of single-layer graphene. *Nano Lett.* 2008, 8, 902-907.
5. Lee, C.; Wei, X. D.; Kysar, J. W.; Hone, J. Measurement of the elastic properties and intrinsic strength of monolayer graphene. *Science* 2008, 321, 385-388.

6. Ho, K. I.; Huang, C. H.; Liao, J. H.; Zhang, W. J.; Li, L. J.; Lai, C. S.; Su, C. Y. Fluorinated Graphene as High Performance Dielectric Materials and the Applications for Graphene Nanoelectronics. *Sci Rep* 2014, 4.
7. Lemme, M. C.; Echtermeyer, T. J.; Baus, M.; Kurz, H. A graphene field-effect device. *IEEE Electron Device Lett.* 2007, 28, 282-284.
8. Becerril, H. A.; Mao, J.; Liu, Z.; Stoltenberg, R. M.; Bao, Z.; Chen, Y. Evaluation of solution-processed reduced graphene oxide films as transparent conductors. *ACS Nano* 2008, 2, 463-470.
9. Matyba, P.; Yamaguchi, H.; Eda, G.; Chhowalla, M.; Edman, L.; Robinson, N. D. Graphene and Mobile Ions: The Key to All-Plastic, Solution-Processed Light-Emitting Devices. *ACS Nano* 2010, 4, 637-642.
10. Eda, G.; Fanchini, G.; Chhowalla, M. Large-area ultrathin films of reduced graphene oxide as a transparent and flexible electronic material. *Nat. Nanotechnol.* 2008, 3, 270-274.
11. Stankovich, S.; Dikin, D. A.; Dommett, G. H. B.; Kohlhaas, K. M.; Zimney, E. J.; Stach, E. A.; Piner, R. D.; Nguyen, S. T.; Ruoff, R. S. Graphene-based composite materials. *Nature* 2006, 442, 282-286.
12. Kakaei, K.; Zhiani, M. A new method for manufacturing graphene and electrochemical characteristic of graphene-supported Pt nanoparticles in methanol oxidation. *Journal of Power Sources* 2013, 225, 356-363.
13. Liu, C. G.; Yu, Z. N.; Neff, D.; Zhamu, A.; Jang, B. Z. Graphene-Based Supercapacitor with an Ultrahigh Energy Density. *Nano Lett.* 2010, 10, 4863-4868.
14. Yoo, E.; Kim, J.; Hosono, E.; Zhou, H.; Kudo, T.; Honma, I. Large reversible Li storage of graphene nanosheet families for use in rechargeable lithium ion batteries. *Nano Lett.* 2008, 8, 2277-2282.
15. Yan, Z.; Liu, G. X.; Khan, J. M.; Balandin, A. A. Graphene quilts for thermal management of high-power GaN transistors. *Nat. Commun.* 2012, 3.
16. Shao, Y. Y.; Wang, J.; Wu, H.; Liu, J.; Aksay, I. A.; Lin, Y. H. Graphene Based Electrochemical Sensors and Biosensors: A Review. *Electroanalysis* 2010, 22, 1027-1036.
17. Martinez, A.; Fuse, K.; Yamashita, S. Mechanical exfoliation of graphene for the passive mode-locking of fiber lasers. *Appl. Phys. Lett.* 2011, 99.
18. Su, C. Y.; Lu, A. Y.; Wu, C. Y.; Li, Y. T.; Liu, K. K.; Zhang, W. J.; Lin, S. Y.; Juang, Z. Y.; Zhong, Y. L.; Chen, F. R.; Li, L. J. Direct Formation of Wafer Scale Graphene Thin Layers on Insulating Substrates by Chemical Vapor Deposition. *Nano Lett.* 2011, 11, 3612-3616.
19. Yu, Q. K.; Jauregui, L. A.; Wu, W.; Colby, R.; Tian, J. F.; Su, Z. H.; Cao, H. L.; Liu, Z. H.; Pandey, D.; Wei, D. G.; Chung, T. F.; Peng, P.; Guisinger, N. P.; Stach, E. A.; Bao, J. M.; Pei, S. S.; Chen, Y. P. Control and characterization of individual grains and grain boundaries in graphene grown by chemical vapour deposition. *Nat. Mater.* 2011, 10, 443-449.
20. Reina, A.; Jia, X. T.; Ho, J.; Nezich, D.; Son, H. B.; Bulovic, V.; Dresselhaus, M. S.; Kong, J. Large Area, Few-Layer Graphene Films on Arbitrary Substrates by Chemical Vapor Deposition. *Nano Lett.* 2009, 9, 30-35.
21. Huang, H.; Chen, W.; Chen, S.; Wee, A. T. S. Bottom-up Growth of Epitaxial Graphene on 6H-SiC(0001). *ACS Nano* 2008, 2, 2513-2518.

22. Paton, K. R.; Varrla, E.; Backes, C.; Smith, R. J.; Khan, U.; O'Neill, A.; Boland, C.; Lotya, M.; Istrate, O. M.; King, P.; Higgins, T.; Barwich, S.; May, P.; Puczkarski, P.; Ahmed, I.; Moebius, M.; Pettersson, H.; Long, E.; Coelho, J.; O'Brien, S. E.; McGuire, E. K.; Sanchez, B. M.; Duesberg, G. S.; McEvoy, N.; Pennycook, T. J.; Downing, C.; Crossley, A.; Nicolosi, V.; Coleman, J. N. Scalable production of large quantities of defect-free few-layer graphene by shear exfoliation in liquids. *Nat. Mater.* 2014, 13, 624-630.
23. Hernandez, Y.; Nicolosi, V.; Lotya, M.; Blighe, F. M.; Sun, Z. Y.; De, S.; McGovern, I. T.; Holland, B.; Byrne, M.; Gun'ko, Y. K.; Boland, J. J.; Niraj, P.; Duesberg, G.; Krishnamurthy, S.; Goodhue, R.; Hutchison, J.; Scardaci, V.; Ferrari, A. C.; Coleman, J. N. High-yield production of graphene by liquid-phase exfoliation of graphite. *Nat. Nanotechnol.* 2008, 3, 563-568.
24. Zhu, Y. W.; Murali, S.; Cai, W. W.; Li, X. S.; Suk, J. W.; Potts, J. R.; Ruoff, R. S. Graphene and Graphene Oxide: Synthesis, Properties, and Applications. *Adv. Mater.* 2010, 22, 3906-3924.
25. Dreyer, D. R.; Park, S.; Bielawski, C. W.; Ruoff, R. S. The chemistry of graphene oxide. *Chem. Soc. Rev.* 2010, 39, 228-240.
26. Leon, V.; Rodriguez, A. M.; Prieto, P.; Prato, M.; Vazquez, E. Exfoliation of Graphite with Triazine Derivatives under Ball-Milling Conditions: Preparation of Few-Layer Graphene via Selective Noncovalent Interactions. *ACS Nano* 2014, 8, 563-571.
27. Li, X. L.; Zhang, G. Y.; Bai, X. D.; Sun, X. M.; Wang, X. R.; Wang, E.; Dai, H. J. Highly conducting graphene sheets and Langmuir-Blodgett films. *Nat. Nanotechnol.* 2008, 3, 538-542.
28. Su, C. Y.; Xu, Y. P.; Zhang, W. J.; Zhao, J. W.; Tang, X. H.; Tsai, C. H.; Li, L. J. Electrical and Spectroscopic Characterizations of Ultra-Large Reduced Graphene Oxide Monolayers. *Chem. Mat.* 2009, 21, 5674-5680.
29. Su, C. Y.; Xu, Y. P.; Zhang, W. J.; Zhao, J. W.; Liu, A. P.; Tang, X. H.; Tsai, C. H.; Huang, Y. Z.; Li, L. J. Highly Efficient Restoration of Graphitic Structure in Graphene Oxide Using Alcohol Vapors. *ACS Nano* 2010, 4, 5285-5292.
30. Abdelkader, A. M.; Cooper, A. J.; Dryfe, R. A. W.; Kinloch, I. A. How to get between the sheets: a review of recent works on the electrochemical exfoliation of graphene materials from bulk graphite. *Nanoscale* 2015, 7, 6944-6956.
31. Najafabadi, A. T.; Gyenge, E. High-yield graphene production by electrochemical exfoliation of graphite: Novel ionic liquid (IL)-acetonitrile electrolyte with low IL content. *Carbon* 2014, 71, 58-69.
32. Parvez, K.; Wu, Z. S.; Li, R. J.; Liu, X. J.; Graf, R.; Feng, X. L.; Mullen, K. Exfoliation of Graphite into Graphene in Aqueous Solutions of Inorganic Salts. *J. Am. Chem. Soc.* 2014, 136, 6083-6091.
33. Lu, J.; Yang, J. X.; Wang, J. Z.; Lim, A. L.; Wang, S.; Loh, K. P. One-Pot Synthesis of Fluorescent Carbon Nanoribbons, Nanoparticles, and Graphene by the Exfoliation of Graphite in Ionic Liquids. *ACS Nano* 2009, 3, 2367-2375.
34. Su, C. Y.; Lu, A. Y.; Xu, Y. P.; Chen, F. R.; Khlobystov, A. N.; Li, L. J. High-Quality Thin Graphene Films from Fast Electrochemical Exfoliation. *ACS Nano* 2011, 5, 2332-2339.

35. Kakaei, K. One-pot electrochemical synthesis of graphene by the exfoliation of graphite powder in sodium dodecyl sulfate and its decoration with platinum nanoparticles for methanol oxidation. *Carbon* 2013, 51, 195-201.
36. Kakaei, K.; Hasanpour, K. Synthesis of graphene oxide nanosheets by electrochemical exfoliation of graphite in cetyltrimethylammonium bromide and its application for oxygen reduction. *Journal of Materials Chemistry A* 2014, 2, 15428-15436.
37. Krauss, B.; Lohmann, T.; Chae, D. H.; Haluska, M.; von Klitzing, K.; Smet, J. H. Laser-induced disassembly of a graphene single crystal into a nanocrystalline network. *Phys. Rev. B* 2009, 79.
38. Graf, D.; Molitor, F.; Ensslin, K.; Stampfer, C.; Jungen, A.; Hierold, C.; Wirtz, L. Spatially resolved raman spectroscopy of single- and few-layer graphene. *Nano Lett.* 2007, 7, 238-242.
39. Ferrari, A. C.; Meyer, J. C.; Scardaci, V.; Casiraghi, C.; Lazzeri, M.; Mauri, F.; Piscanec, S.; Jiang, D.; Novoselov, K. S.; Roth, S.; Geim, A. K. Raman spectrum of graphene and graphene layers. *Phys. Rev. Lett.* 2006, 97.
40. Malard, L. M.; Pimenta, M. A.; Dresselhaus, G.; Dresselhaus, M. S. Raman spectroscopy in graphene. *Phys. Rep.-Rev. Sec. Phys. Lett.* 2009, 473, 51-87.
41. Ferrari, A. C. Raman spectroscopy of graphene and graphite: Disorder, electron-phonon coupling, doping and nonadiabatic effects. *Solid State Commun.* 2007, 143, 47-57.
42. Cancado, L. G.; Pimenta, M. A.; Neves, B. R. A.; Dantas, M. S. S.; Jorio, A. Influence of the atomic structure on the Raman spectra of graphite edges. *Phys. Rev. Lett.* 2004, 93.
43. Buglione, L.; Chng, E. L. K.; Ambrosi, A.; Sofer, Z.; Pumera, M. Graphene materials preparation methods have dramatic influence upon their capacitance. *Electrochem. Commun.* 2012, 14, 5-8.
44. Lucchese, M. M.; Stavale, F.; Ferreira, E. H. M.; Vilani, C.; Moutinho, M. V. O.; Capaz, R. B.; Achete, C. A.; Jorio, A. Quantifying ion-induced defects and Raman relaxation length in graphene. *Carbon* 2010, 48, 1592-1597.
45. Cancado, L. G.; Jorio, A.; Ferreira, E. H. M.; Stavale, F.; Achete, C. A.; Capaz, R. B.; Moutinho, M. V. O.; Lombardo, A.; Kulmala, T. S.; Ferrari, A. C. Quantifying Defects in Graphene via Raman Spectroscopy at Different Excitation Energies. *Nano Lett.* 2011, 11, 3190-3196.
46. Cancado, L. G.; Takai, K.; Enoki, T.; Endo, M.; Kim, Y. A.; Mizusaki, H.; Jorio, A.; Coelho, L. N.; Magalhaes-Paniago, R.; Pimenta, M. A. General equation for the determination of the crystallite size L_a of nanographite by Raman spectroscopy. *Appl. Phys. Lett.* 2006, 88.
47. Feng, H. B.; Cheng, R.; Zhao, X.; Duan, X. F.; Li, J. H. A low-temperature method to produce highly reduced graphene oxide. *Nat. Commun.* 2013, 4.
48. Gunes, F.; Shin, H. J.; Biswas, C.; Han, G. H.; Kim, E. S.; Chae, S. J.; Choi, J. Y.; Lee, Y. H. Layer-by-Layer Doping of Few-Layer Graphene Film. *ACS Nano* 2010, 4, 4595-4600.

49. Kim, H.; Abdala, A. A.; Macosko, C. W. Graphene/Polymer Nanocomposites. *Macromolecules* 2010, 43, 6515-6530.

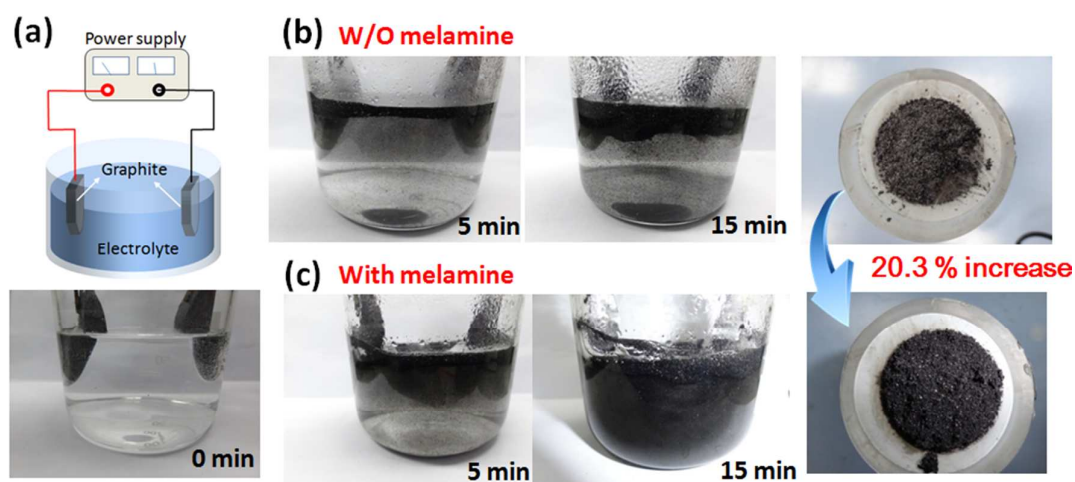


Figure 1. (a) Schematic illustration of the setup and image of the electrochemical exfoliation of graphite. (b)(c) Images of the process evolution of electrochemical exfoliation from graphite for the cases of the electrolyte with and without melamine additives, respectively.

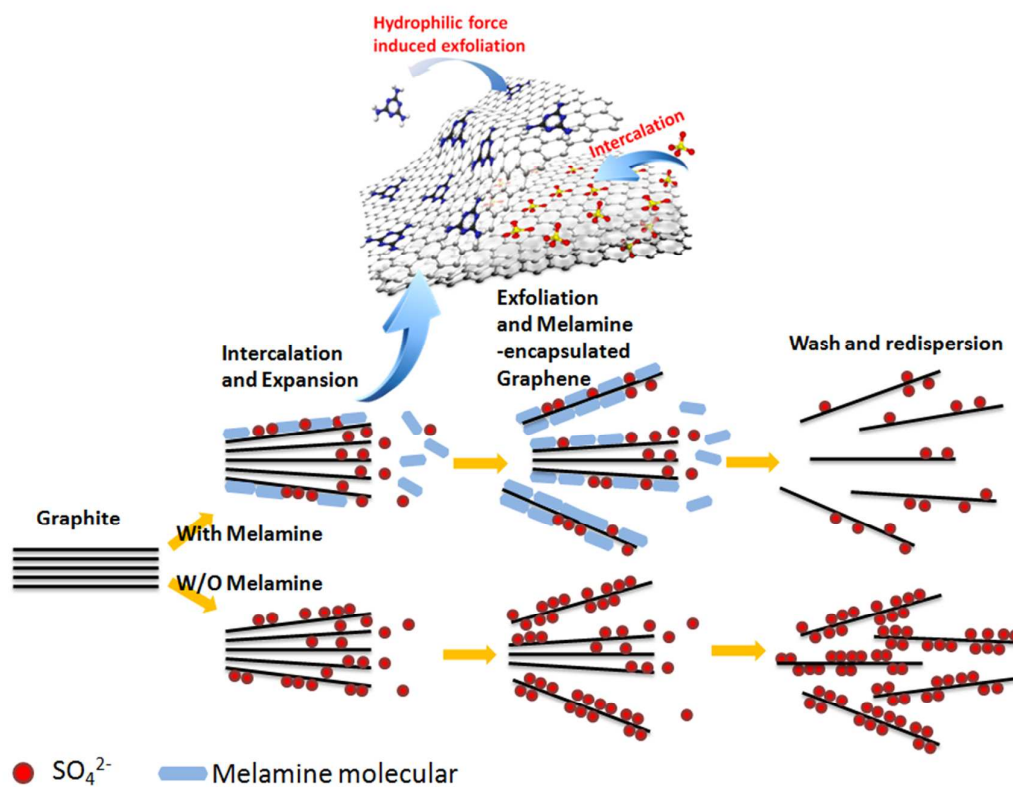


Figure 2. The schematic illustration of the mechanisms for the electrochemical exfoliation of graphite with/without melamine additives. For the case of melamine additives, the as-exfoliated graphene sheets were *insitu* encapsulated with melamine molecules, thereby preventing further oxidation from the acid species.

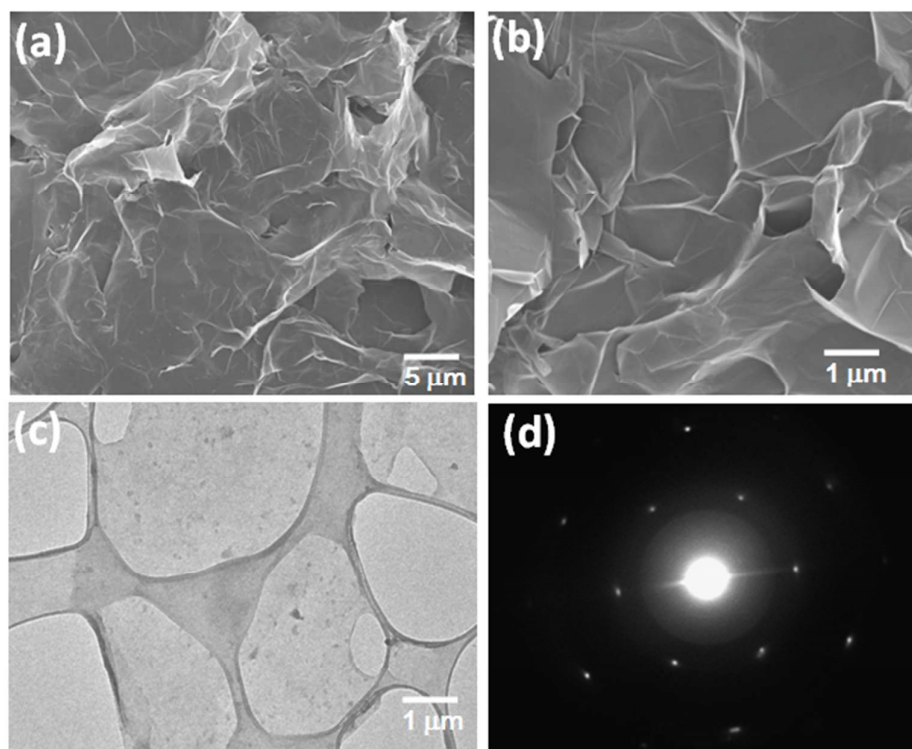


Figure 3. (a) SEM image of the surface morphology for the exfoliated graphene sheets from graphite with the use of melamine additives during electrochemical exfoliation. (b) The magnified images of (a). (c) The TEM image of a graphene sheet. (d) The diffraction pattern of the graphene sheet taken from (c), indicating one set of the typical six-fold symmetric diffraction pattern of the graphene lattice.

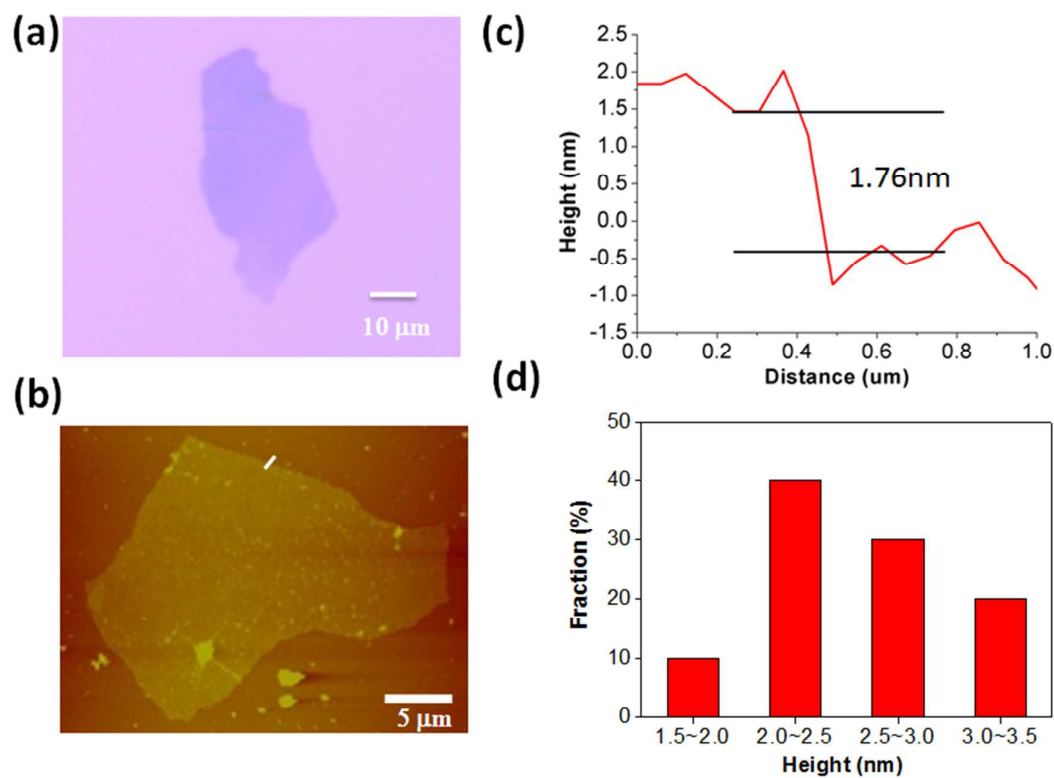


Figure 4. (a) The typical optical image of a graphene sheet on a SiO₂ substrate. (b) The typical AFM image of an exfoliated thin graphene sheet. (c) The corresponding AFM height profile for a graphene sheet in (b) (~1.76 nm in thickness). (d) Histogram of the statistical thickness analysis for the exfoliated graphene sheets of 47 randomly selected sheets characterized using AFM measurements.

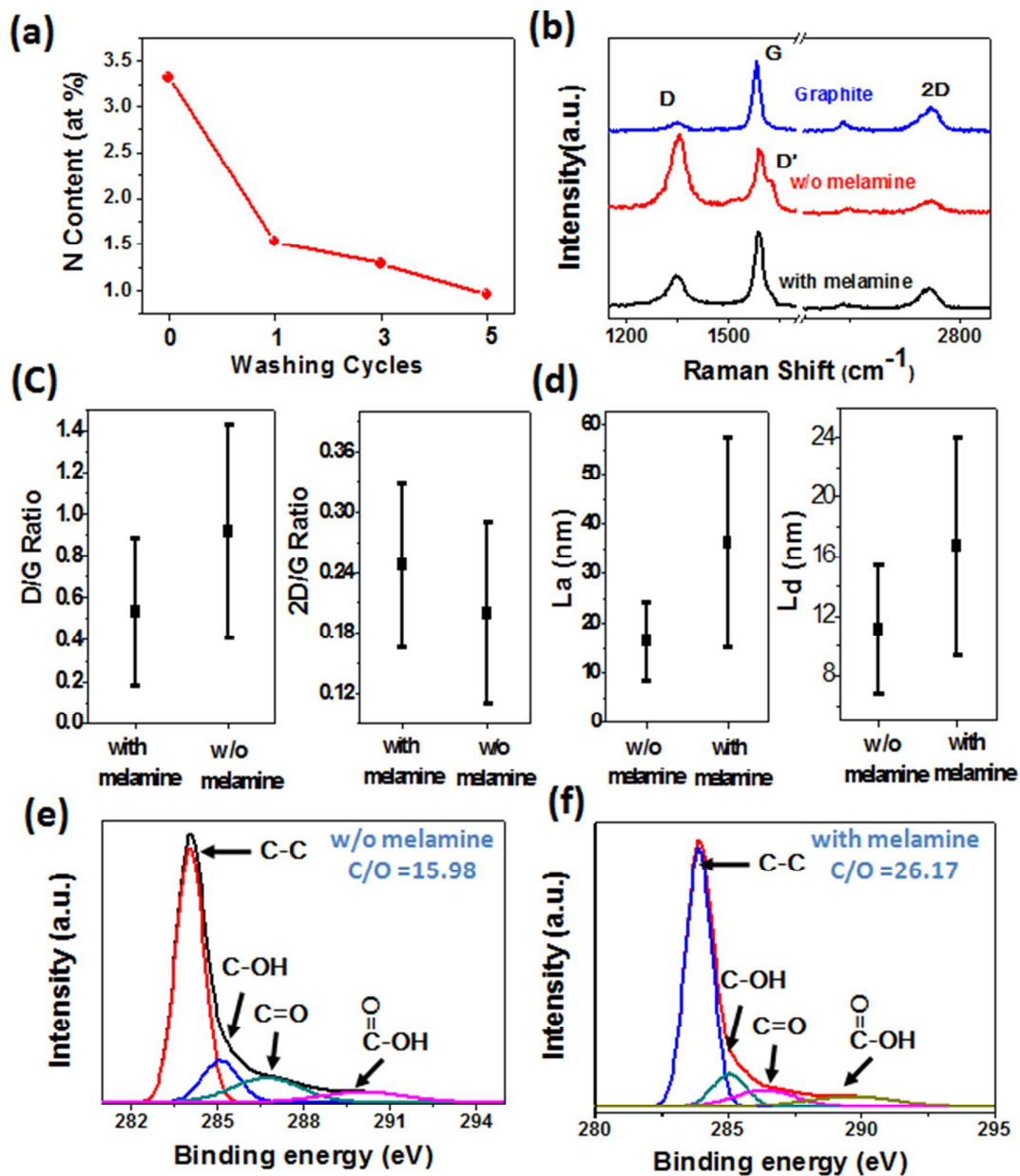


Figure 5. (a) The correlation of nitrogen contamination and water flush cycling. (b) The Raman spectra for graphite and as-exfoliated graphene with and without melamine additives. (c) Comparison of the Raman D/G and 2D/G ratios for the cases of the electrolyte with and without melamine additives. (d) The estimated graphene crystallite size (L_a) and the distance between defects (L_d) for the cases with and without melamine

additives. (e) and (f) XPS C1s spectra for graphene without and with melamine additives, respectively. The inset shows the corresponding C/O ratio.

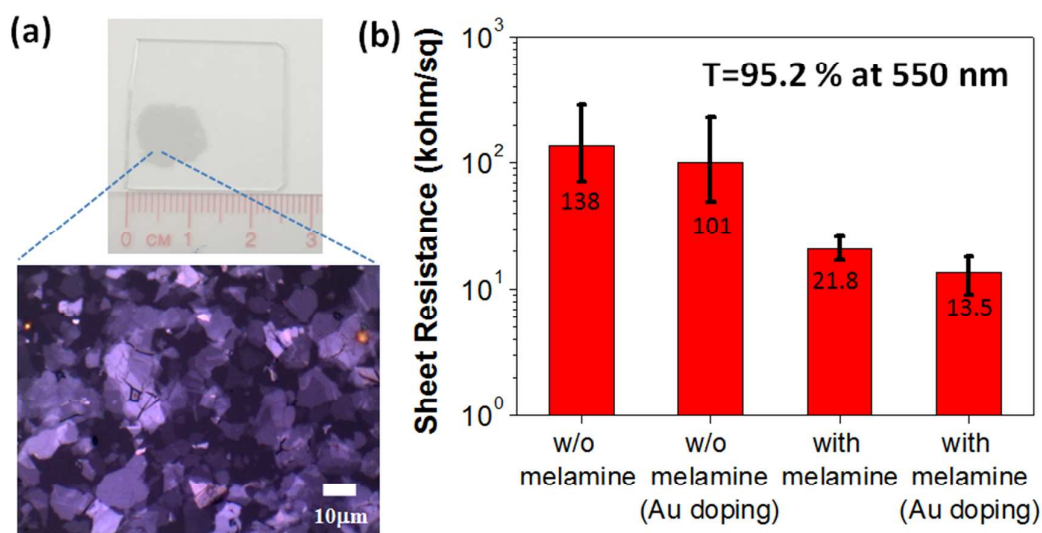


Figure 6 (a) The optical image of the graphene self-assembled percolation film. (b) Statistical ensemble sheet resistance data for graphene films made from various conditions. The data are selected for the graphene film with optical transmittance of ~95.2 % at 550 nm.

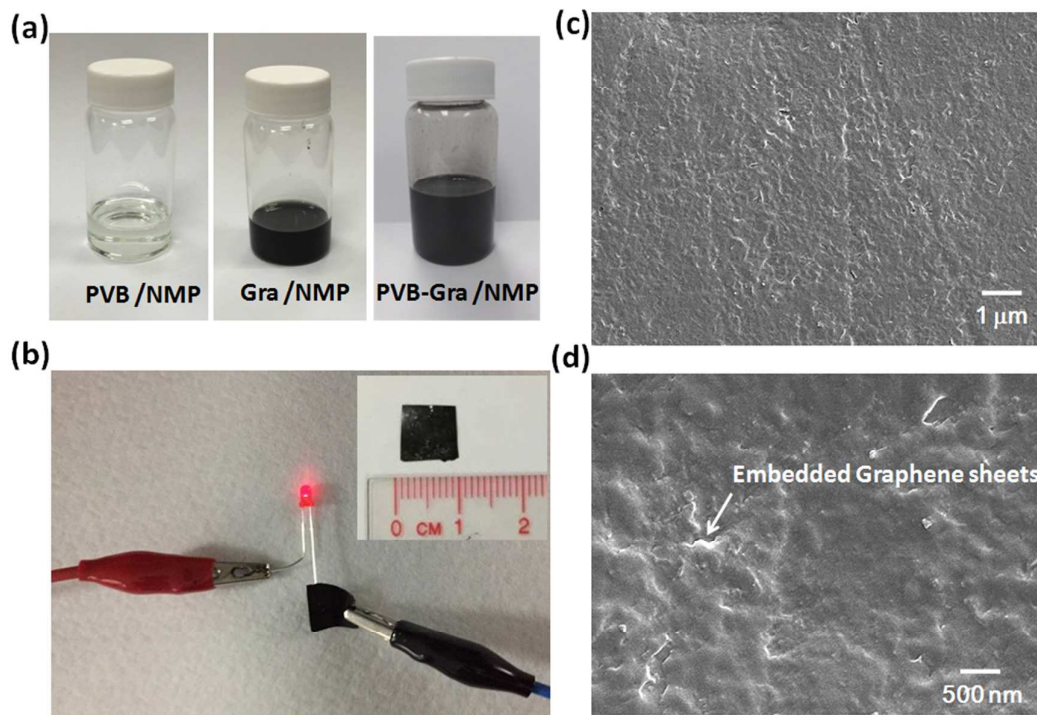


Figure 7 (a) Images of the PVB and graphene in NMP suspensions as well as the mixture of both solutions. (b) The prepared graphene/PVB composite film exhibits electrical conductivity. The inset is the image for this composite film. (c) The SEM image on graphene/PVB composite film. (d) The enlarged image indicating the graphene sheets well dispersed and embedded in matrix polymer.

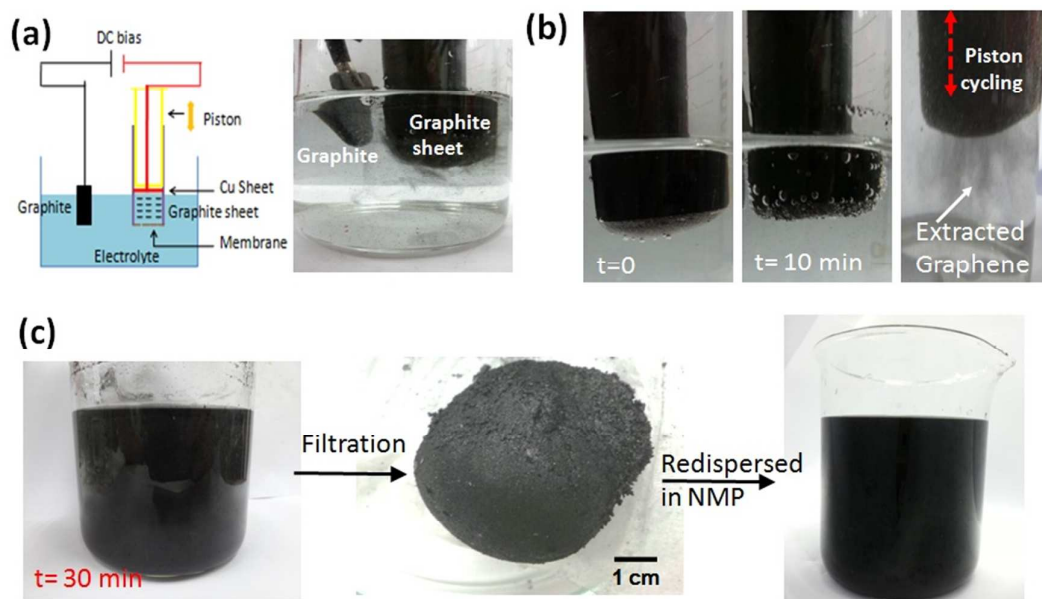


Figure 8. Concept of the continuous production of graphene. (a) Illustration of the scheme and image of the facility setup where the piston-operated cylinder was loaded with graphite flake powders for the electrochemical exfoliation process. (b) The evolution during the exfoliation process. After 10 min of processing, the applied voltage was turned off. Next, piston cycling was performed to extract the exfoliated graphene flakes. (c) The photo image of the obtained graphene powder and its suspension in NMP solution.